Available online at www.sciencedirect.com

ScienceDirect

IFAC Papers Online CONFERENCE PAPER ARCHIVE

IFAC-PapersOnLine 49-26 (2016) 264–269

Quantitative comparison of competing PDE models for Pom1p dynamics in fission yeast ⋆

Sabrina Hross†, Anna Fiedler†, Fabian J. Theis, Jan Hasenauer

Institute of Computational Biology, Helmholtz Zentrum München – German Research Center for Environmental Health, München, Germany. & Chair of Mathematical Modeling of Biological Systems, Technische Universität München, München, Germany.

Abstract: Gradient formation of Pom1 is a key regulator of cell cycle and cell growth in fission yeast (Schizosaccharomyces pombe). A variety of models to explain Pom1 gradient formation have been proposed, a quantitative analysis and comparison of these models is, however, still missing. In this work we present four models from the literature and perform a quantitative comparison using published single-cell images of the gradient formation process. For the comparison of these partial differential equation (PDE) models we use state-of-the-art techniques for parameter estimation together with model selection. The model selection supports the hypothesis that buffering of the gradient is achieved via clustering. The selected model does, however, not ensure mass conservation, which might be considered as problematic.

Keywords: systems biology, partial differential equation, parameter estimation, gradient formation, Pom1 signaling

1. INTRODUCTION

The size of a cell can have a strong effect on intracellular processes (Farnier et al., 2003). The precise mechanisms by which cells control their size and achieve cell size homeostasis is however still poorly understood (Taheri-Araghi et al., 2015). For the model organism fission yeast *Schizosaccharomyces pombe* it has been established that Pom1 plays an essential role (Almeida and Tyers, 2009; Moseley et al., 2009; Martin and Berthelot-Grosjean, 2009). Fission yeast is a rod shaped eucaryotic cell, which divides along the middle axis to form two daughter cells. It has been discovered that the polarity factor Pom1 forms a gradient in the cell membranes. Its concentration is highest at the tips and decreases towards the cell middle. As long as the cell is still small Pom1 inhibits the cell division mechanism positioned at the cell middle. When the cell grows, however, the concentration of Pom1 at the division axis in the middle of the cell decreases and the cell division machinery becomes activated. See Figure 1A for a schematic of the process.

While the general role of Pom1 in gradient formation was confirmed by knock-out experiments the detailed mechanism behind the formation and the stabilization of the gradient against noise and fluctuations in the Pom1 concentration at the tips of the cell remains unclear. A minimal model that does not describe the stabilization against noise was introduced by Saunders et al. (2012). Subsequently, three mechanisms were proposed for the formation of the Pom1 gradient and its stabilization against fluctuations: cluster formation (Saunders et al., 2012; Saunders, 2015), autophosphorylation (Hachet et al., 2011, 2012) and transphosphorylation (Hersch et al., 2015). Figure 1 provides schematics for all four models. While all models could reproduce some qualitative properties of Pom1 gradient formation, a quantitative comparison is missing.

To compare the spatio-temporal models of Pom1 gradient formation, we used published single-cell imaging data. We estimated the parameters of all models via maximum likelihood methods. To ensure efficiency and reliability, we employed state-of-the-art numerical schemes, providing forward sensitivities. The parameter estimation results are employed for model selection, providing insights into the relevance of different mechanisms. Our study provides the first quantitative evaluation of models proposed in several studies, providing an essential step towards a mechanistic understanding of the process.

2. MATHEMATICAL MODELING

We consider four different models for Pom1 gradient formation:

- the minimal description by the **source-diffusion degradation model (SDD)** (Saunders et al., 2012);
- the **non-linear cluster formation model (NLIC)** (Saunders et al., 2012);
- the **autophosphorylation model (AP)** (Hachet et al., 2011); and
- the **multiple site phosphorylation model (MSP)** (Hersch et al., 2015).

⋆ The authors acknowledge financial support from the Postdoctoral Fellowship Program (PFP) of the Helmholtz Zentrum München.
† Both authors contributed equally.

10.1016/j.ifacol.2016.12.136

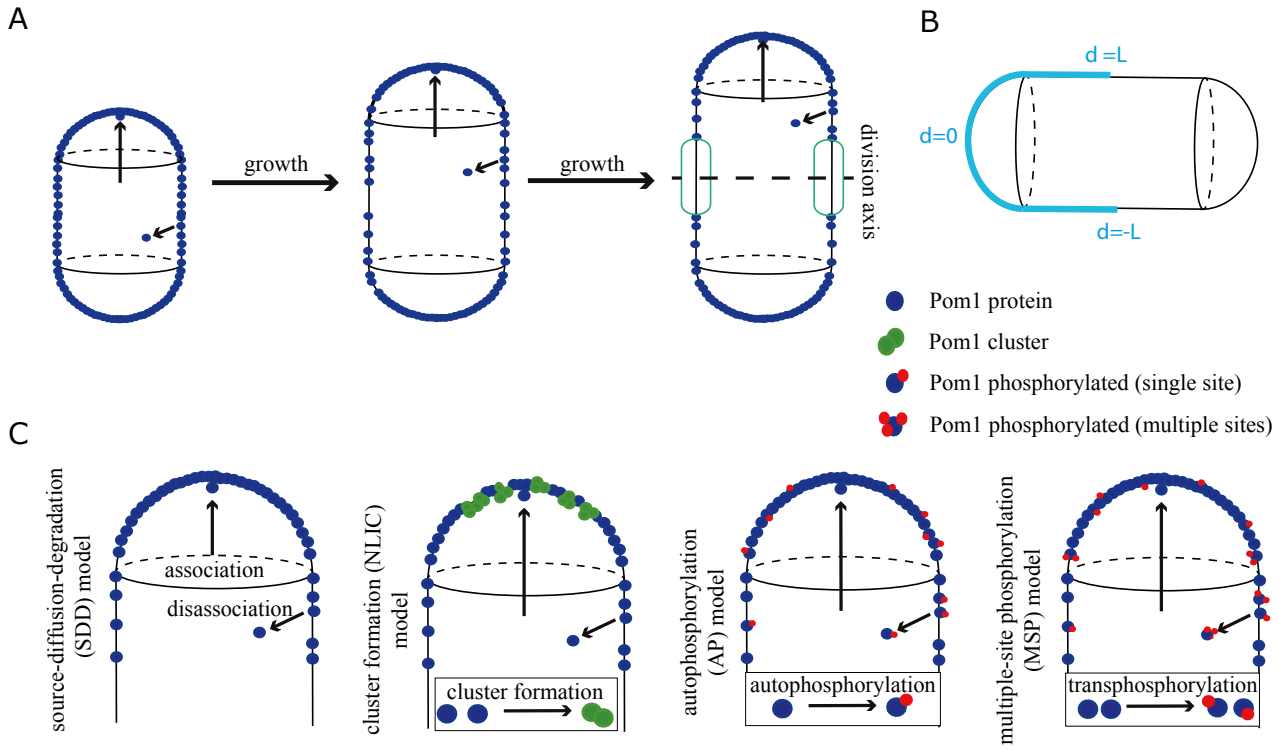

Fig. 1. **Schematic of the Pom1 model.** A) Cell size control in fission yeast. The gradient from the tips is constant and if the cell grows the concentration at the cell middle reduces until a region with low concentration arises. This is where division will take place. B) Schematic of the fission yeast geometry. Along the cyan line the models are considered. C) Schematic of the four Pom1 gradient formation models considered. All share the same process of association and disassociation but differ regarding cluster formation or phosphorylation processes.

All models assume that the cells have a rod shape and are symmetrical with respect to the horizontal and vertical axis, hence, a cylindrical body with half spheres as tips is considered. The gradient formation is modeled along one line on the surface with spatial position $d \in \Omega = [-L, L]$ and length $L = 7\mu m$ (Figure 1B). Analogously to Hachet et al. (2011), we discretize the process on a line of the surface of the cell. This enables us to simulate the whole tip region in one step, in contrast to (Saunders et al., 2012) where the singularity due to the projection had to be treated by artificial boundary conditions. The units used in the following equations are micrometers (μm), seconds (s), mol and units of fluorescence intensity (UI).

Source-diffusion-degradation (SDD) model. In the SDD model by Saunders et al. (2012) Pom1 associates to the cell membrane in a circular region at the tip of the cell, i.e., at $d = 0$ (see Figure 1). The rate of molecule binding is denoted by J, and the association frequency at point $d \in \Omega$ is assumed to follow a Gaussian distribution with mean zero and width ρ. Once associated to the membrane Pom1 diffuses along the membrane with diffusion constant D and disassociates with rate μ. The resulting PDE model is given by

$$\frac{\partial u}{\partial t} = D\frac{\partial^2 u}{\partial d^2} - \mu u + \frac{J}{\sqrt{2\pi}\rho} e^{-d^2/2\rho^2} \tag{1}$$

for $d \in \Omega$ and parameter $\theta = (D, \mu, J, \rho)^T$.

Non-linear interacting cluster formation (NLIC) model. The NLIC model proposed by Saunders et al. (2012) assumes that the Pom1 gradient is stabilized against fluctuations in the input rate by cluster formation, i.e., the formation of a fast and a slow moving Pom1 component which is formed by non-linear interaction of both. Following the model, Pom1 can either occur as fast moving single molecules denoted by u or as slow moving clusters denoted by u_c. Both types of Pom1, u and u_c, diffuse along the cell membrane with diffusion constants D and D_c, respectively. Slow clusters are assumed to form mainly at the tips, which is also the space where most of the association of single molecules happens. A fraction ε of the Pom1 associated to the membrane at the tips are single molecules and the other fraction of $1-\varepsilon$ are clusters. It is assumed that only single molecules can disassociate from the membrane with rate μ. Saunders et al. (2012) assume that a single molecule becomes part of a cluster with rate β. A cluster fragments into the single molecule state with rate α. Hence, the model is given by

$$\begin{aligned}\frac{\partial u}{\partial t} &= D\frac{\partial^2 u}{\partial d^2} + \alpha u_c - \beta u u_c - \mu u + \varepsilon \frac{J}{\sqrt{2\pi}\rho} e^{-d^2/2\rho^2} \\ \frac{\partial u_c}{\partial t} &= D_c\frac{\partial^2 u_c}{\partial d^2} - \alpha u_c + \beta u u_c + (1-\varepsilon)\frac{J}{\sqrt{2\pi}\rho} e^{-d^2/2\rho^2}\end{aligned} \tag{2}$$

for $d \in \Omega$ and parameter $\theta = (D, D_c, \mu, \alpha, \beta, J, \rho, \varepsilon)^T$. The diffusion coefficient of the Pom1 clusters is parameterized as fraction $\xi_c \leq 1$ of the diffusion coefficient of free Pom1, $D_c = \xi_c D$. A weakness of this model is that it does not ensure mass conservation of Pom1 molecules in

the membrane. Clusters with more than two molecule are transformed to a single molecule upon fragmentation.

Autophosphorylation (AP) model. The AP model was introduced by Hachet et al. (2011) and considers slow diffusing phosphorylated, u_p, and fast diffusing unphosphorylated, u, forms of Pom1. In this model Pom1 is associated to the membrane in unphosphorylated form and autophosphorylates with rate α. The phosphorylated form disassociates from the membrane with rate μ. The phosphorylated and unphosphorylated forms have diffusion constants D_p and D, respectively. This yields the model

$$\begin{aligned} \frac{\partial u}{\partial t} &= D\frac{\partial^2 u}{\partial d^2} - \alpha u + \frac{J}{\sqrt{2\pi}\rho} e^{-d^2/2\rho^2} \\ \frac{\partial u_p}{\partial t} &= D_p \frac{\partial^2 u_p}{\partial d^2} + \alpha u - \mu u_p \end{aligned} \tag{3}$$

with $d \in \Omega$, $\theta = (D, D_p, \mu, \alpha, J, \rho)^T$ and $D_p = \xi_p D$ with $\xi_p \leq 1$.

Multiple-site phosphorylation (MSP) model. The MSP model was introduced by Hersch et al. (2015). In contrast to the AP model, Pom1 is assumed to be phosphorylated at multiple phosphorylation sites (up to 6 possible sites have been found in Pom1 (Hachet et al., 2011)). The phosphorylation is acquired via transphosphorylation, i.e., two Pom1 molecules meet and phosphorylate each other with rate α. The full model considers eight Pom1 species. Hersch et al. (2015) reduced the model and showed that a one dimensional model with concentration depended disassociation is a good approximation to the full model. Following Hersch et al. (2015), we consider the model

$$\frac{\partial u}{\partial t} = D\frac{\partial^2 u}{\partial d^2} - \alpha u^2 + \frac{J}{\sqrt{2\pi}\rho} e^{-d^2/2\rho^2} \tag{4}$$

for $d \in \Omega$ and with parameters $\theta = (D, \alpha, J, \rho)^T$.

Initial and boundary conditions. We assume no-flux boundary conditions at the division axis of the cells for all biochemical species. In the unperturbed system, the initial conditions for all biochemical species are assumed to be in steady state. For FRAP experiments (see description below), the species are zero in the bleached region $Q \subseteq \Omega$, e.g.

$$u(0, d) = \begin{cases} 0 & \text{for } d \in Q \\ u^\infty(d; \theta) & \text{otherwise} \end{cases} \tag{5}$$

where $u^\infty(d; \theta)$ denotes the steady state of the model considered for parameter θ.

Numerical simulation. For numerical simulation of the PDE models, we employed the method of lines. The systems of ODEs are implemented in MATLAB and compiled and simulated using AMICI (Kazeroonian et al., 2016). AMICI provides an interface to the SUNDIALS solver suite (Hindmarsh et al., 2005). As the numerical simulation using AMICI was computationally efficient and robust, we also used it to compute the steady state of the models.

3. PARAMETER ESTIMATION AND MODEL SELECTION

To select the best suited model of Pom1 gradient formation, we assess the capability of the models to describe the available experimental data. We use maximum likelihood estimation to infer the unknown parameters. The likelihood function, $L(\theta)$, describes the conditional probability of observing the data given a particular set of model parameters. For numerical reasons the negative log-likelihood, $J(\theta) = -\log(L(\theta))$, is minimized to find the maximum likelihood estimator (MLE),

$$\hat{\theta} = \arg\min_\theta J(\theta). \tag{6}$$

In the following, we will present the measurement data considered and the negative log-likelihood function.

3.1 Measurement data

We use the single-cell imaging data collected by Saunders et al. (2012), the only publicly available dataset regarding Pom1 gradient formation. These experimental data were obtained by fluorescent labeling of Pom1. Saunders et al. (2012) reported:

- the intensity profile along the membrane in the unperturbed system,
- the fluorescence recovery after photobleaching of the full and the half tip; and
- the total protein abundance.

For the detailed experimental methods and measurement techniques we refer the reader to the original work of Saunders et al. (2012).

All experiments provide information about the total Pom1 concentration, $u_{\text{tot}}(d, t)$. As SDD and MSP each only consider one form of Pom1, u_{tot} corresponds directly to u. NLIC and AP consider additionally u_c and u_p, respectively. The clusters in u_c consist of an undetermined number of Pom1 molecules. To account for this we introduce scaling factor s_c, that can be interpreted as the average cluster size and can range between one and the maximal cluster size of 200 (Saunders, 2015), i.e., $1 < s_c < 200$. This scaling factor is estimated from the data as well. Accordingly, we get

$$u_{\text{tot}}(d, t; \theta) = \begin{cases} u(d, t; \theta) + s_c u_c(d, t; \theta) & \text{for NLIC} \\ u(d, t; \theta) + u_p(d, t; \theta) & \text{for AP} \\ u(d, t; \theta) & \text{for SDD, MSP.} \end{cases} \tag{7}$$

In the following, we describe each of the four datasets.

Mean intensity curves. For the mean intensity curves, cells were imaged and for each cell a cortical mask, i.e., a line along the cell membrane, was defined. Along this mask the Pom1 intensities were measured. Measurements were taken at 60 equally spaced spatial points with $d_k \in \Omega$, $k = 1, \ldots, 60$. For each point the normalized mean $\overline{y}_{1,k}$ and the standard error of the mean (SEM) $\overline{\sigma}^2_{1,k}$ were assessed. We introduced an additional scaling factor s_1 to account for the normalization. The observation for normalized mean intensity curves is given by

$$y_{1.k}(\theta) = s_1 u^\infty_{\text{tot}}(d_k; \theta), \text{ for } k = 1, \ldots, 60 \tag{8}$$

with u_{tot}^{∞} denoting the stationary limit of u_{tot}. We consider here the stationary limit as the system is measured in the absence of perturbations.

FRAP measurements. To assess the dynamics of the process, two fluorescence recovery after photobleaching experiments were performed. In the first experiment, the full tip ($Q_2 = [-2.75, 2.75]\mu m$) was bleached and cells were imaged for 300 seconds. In the second experiment only one half tip ($Q_3 = [0, 2.75]\mu m$) was bleached and cells were imaged for 60 seconds. Based on those images the mean recovery curves of the intensity, $\{\overline{y}_{2,k}\}_{k=1}^{10}$ and $\{\overline{y}_{3,k}\}_{k=1}^{20}$, and the standard error of the mean in the bleaching region was calculated for both (see Figure 2D). For parameter estimation we calculated the overall intensity in the predefined bleaching region $d \in Q_i$ at each time point from the model. We assumed that the fluorescence intensity scales linearly with the concentration of Pom1. The scaling for those measurements is unknown. We, hence, introduced scaling factors yielding

$$y_{i,k}(\theta) = s_i \int_{Q_i} u_{\text{tot}}(d, t_k; \theta, Q_i) dd, \quad i \in 2, 3 \tag{9}$$

in which $u_{\text{tot}}(d, t; \theta, Q_i)$ denotes the solution of model for initial condition (5) with $Q = Q_i$.

Pom1 protein abundance. The last set of measurements is the total Pom1 protein abundance in each cell. The fluorescence intensities of Rlc1 and Spn4, two other proteins of fission yeast with well known protein abundances, were imaged with the same exposure. Based on the intensities of those reference proteins the total amount, $\overline{y}_4$, of 5000 ± 1900 Pom1 molecules in the cells was estimated (Saunders et al., 2012). For parameter estimation we assumed that the amount of protein is split equally between the tips. Accordingly, the observable is the integral over the tip region,

$$y_4(\theta) = \int_{\Omega} u_{\text{tot}}^{\infty}(d; \theta) dd. \tag{10}$$

3.2 Parameter estimation

To estimate the parameter of the different models from the experimental data, we formulated likelihood functions. Following the law of large numbers, we assumed that the error of the measured mean $\overline{y}_{i,k}$ is normally distributed. The standard deviation of the distribution is set to the empirically determined standard error of mean, $\overline{\sigma}_{i,k}$. The negative log-likelihood function for dataset i is then given as

$$J_i(\theta) = \frac{1}{2} \sum_{k=1}^{n_i} \log(2\pi \overline{\sigma}_{i,k}^2) + \frac{(\overline{y}_{i,k} - y_{i,k}(\theta))^2}{\overline{\sigma}_{i,k}^2}, \tag{11}$$

in which n_i denotes the number of spatial points or the number of time points, respectively. If (1) the numerical simulation failed or (2) the numerical simulation did not yield a steady state for the unperturbed system (steady state condition: $\partial u / \partial t < 10^{-6}$ for $t = 2.5 \cdot 10^5$), we set $J_i(\theta)$ to infinity.

The negative log-likelihood is the sum of the negative log-likelihoods for the individual experiments, yielding the estimation problem

$$\min_{\theta \in \Theta} J(\theta, y) := \sum_{i=1}^{4} J_i(\theta) \tag{12}$$

in which $\Theta \in \mathbb{R}^{n_\theta}$ denotes the parameter regime. The number of parameters n_θ and the parameter regime depend on the model.

To determine the minimum of (12) – the MLE – we performed multi-start local optimization using the Parameter EStimation TOolbox (PESTO) (Hross and Hasenauer, 2016). The starting points for the local optimizations are drawn from a latin hypercube spanning seven orders of magnitude for most parameters. For each of the models we performed the estimation by multi-start local optimization with PESTO, which uses the MATLAB optimization function *fmincon*.

3.3 Model selection

For model selection we employed the Akaike information criterion (AIC) and the Bayesian information criterion (BIC) (Burnham and Anderson, 2002). With the MLE $\hat{\theta}$, the number of parameters n_θ, and the overall number of data points $M = \sum_{i=1}^{4} n_i$, the AIC can be calculated as

$$\text{AIC} = 2J(\hat{\theta}) + 2n_\theta \tag{13}$$

and the BIC as

$$\text{BIC} = 2J(\hat{\theta}) + n_\theta \log(M). \tag{14}$$

Models with smaller AIC and BIC values are preferable. For both criteria we considered a difference of 10 between AIC and BIC values of competing models as substantial.

4. RESULTS

In the following, we describe the results of parameter estimation and model selection for Pom1 gradient formation.

4.1 Model-data comparison

The parameter estimation methods described in Section 3 were used to infer the parameters of the model alternatives. For the SDD and the MSP, we performed 100 local optimizations. Based on the convergence of the multi-starts we concluded that the global optimum was found for both models. The optimization results for all models are visualized in Figure 2A.

The comparison of the data and the best fit reveals that all models, even the simplest, qualitatively reproduce the observed behavior. In particular the distribution of the intensity profiles (Figure 2B) and the overall protein abundance (Figure 2C) are well described.

Also for full and half tip FRAP, the model fit is mostly within the uncertainty of the measurement. For the full tip FRAP it appears however that the model dynamics are slower than suggested by the data. To confirm this, additional data would be required.

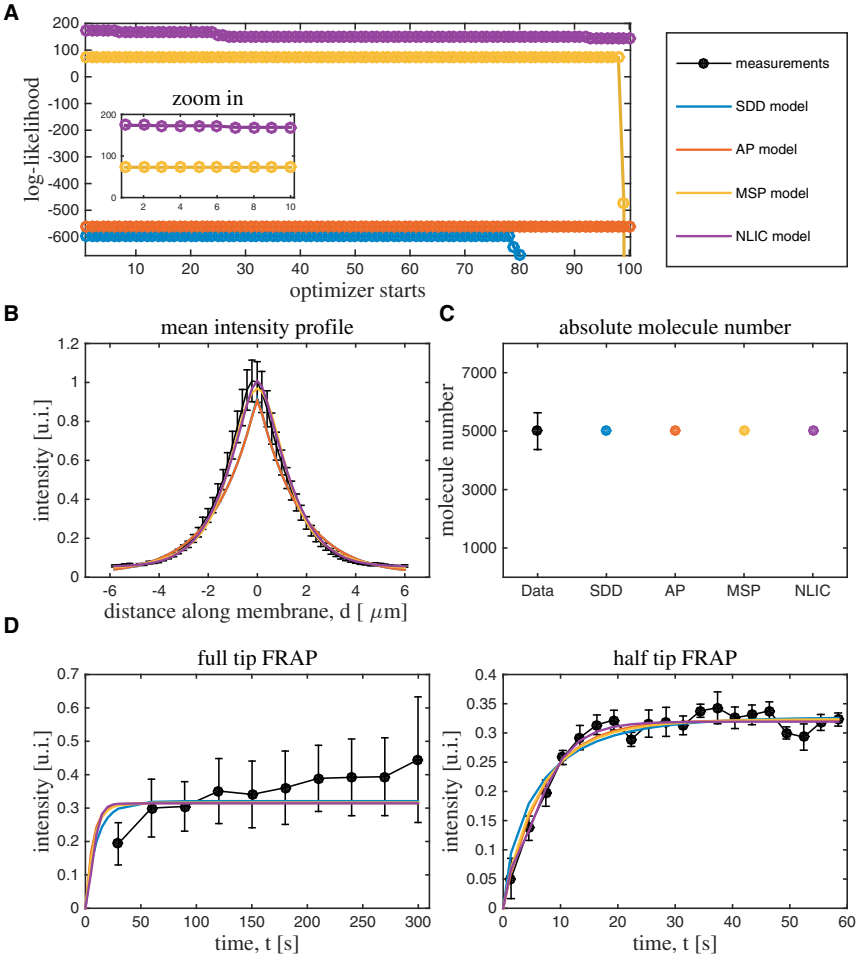

Fig. 2. **Estimation results for Pom1 models.** A) Results of multi-start local optimization. The best 100 optimizer runs are depicted (total number of runs: 100 for SDD and MSP; 500 for AP; 1200 for NLIC). B-D) Measurement and simulation results for B) mean intensity profile, C) total protein abundance and D) half and full tip FRAP recovery curve. The mean of the measured values along with its uncertainty (3 × SEM) is indicated.

Table 1. **Model selection for the Pom1 measurement data.** AIC and BIC values calculated for each model. The model with the lowest AIC/BIC value is selected. A difference between two BIC/AIC values smaller than 10 is considered to be indecisive.

	AIC	ΔAIC	decision	BIC	ΔBIC	decision
Source-diffusion-degradation model (SDD)	1206.3	1529.7	rejected	1223.9	1517.2	rejected
Non-linear interacting cluster formation model (NLIC)	**-323.4**	0	optimal	**-293.2**	0	optimal
Autophosphorylation model (AP)	1142.7	1466.1	rejected	1165.3	1458.6	rejected
Multiple-site phosphorylation model (MSP)	-131.6	191.7	rejected	-114.1	179.2	rejected

4.2 Evaluation of clustering and phosphorylation hypotheses

The results of the multi-starts depicted in Figure 2A already indicated that the SDD and the AP model are outperformed by the NLIC and the MSP model. The evaluation of AIC and BIC revealed that the fit of NLIC is substantially better than that of all other models (Table 4.2).

In summary, we found that a model with clustering as buffering mechanism provides a better description of the considered dataset than the other models.

5. CONCLUSION

Single-cell images combined with fluorescent protein fusions and photobleaching are a widely used tool to study gradient formation in biological processes. The mechanistic mathematical modeling of these data is, however, often challenging as spatial models have to be considered. In this study, we demonstrated that it is feasible using state-of-the-art numerical and optimization methods (see Hock et al. (2013) and references therein).

We considered Pom1 gradient formation, a process for which published data is available. We performed parameter estimation for four competing models, describing different biological hypothesis. The parameter estimation

facilitated the integration of multiple data types and the subsequent model selection. While all models were able to explain the data qualitatively, we found that the NLIC model, incorporating clustering as buffering mechanism, outperformed the other models. Unfortunately, the NLIC model does not ensure mass conservation which might be considered as problematic. Recently, a new cluster formation model was introduced by Saunders (2015), which should be analyzed in future work.

In addition to the consideration of additional mechanistic models, also the statistical description, parameter estimation and model selection can be improved further. We found that the measurement noise of neighboring pixels often appears to be correlated. This correlation could be incorporated into the objective function. Furthermore, differences between individual cells should be assessed in more detail. Complementary, maximum likelihood based methods for parameter estimation and model selection could be replaced by Bayesian methods (Vyshemirsky and Girolami, 2008; Hug et al., 2015). Model selection using Bayes factors (Kass and Raftery, 1995) would for instance account for parameter uncertainties.

In conclusion, we illustrated the importance of rigorous parameter estimation and model selection for the study of spatio-temporal processes. Using these approaches, datasets can be integrated to achieve a coherent picture. Furthermore, the use of statistical approaches promises the reduction of the researcher related bias and the improvement of reproducibility.

REFERENCES

Almeida, R. and Tyers, M. (2009). Cell size control: governed by a spatial gradient. *Developmental Cell*, 17(1), 3–4.

Burnham, K. and Anderson, D. (2002). *Model Selection and Multimodel Inference: A Practical Information-Theoretic Approach (2nd ed)*, volume 172. Springer-Verlag New York, 2nd edition.

Farnier, C., Krief, S., Blache, M., Diot-Dupuy, F., Mory, G., Ferre, P., and Bazin, R. (2003). Adipocyte functions are modulated by cell size change: potential involvement of an integrin/erk signalling pathway. *Int J Obes Relat Metab Disord*, 27(10), 1178–1186.

Hachet, O., Bendezú, F.O., and Martin, S.G. (2012). Fission yeast: in shape to divide. *Current Opinion in Cell Biology*, 24(6), 858–64.

Hachet, O., Berthelot-Grosjean, M., Kokkoris, K., Vincenzetti, V., Moosbrugger, J., and Martin, S.G. (2011). A phosphorylation cycle shapes gradients of the DYRK family kinase Pom1 at the plasma membrane. *Cell*, 145(7), 1116–28.

Hersch, M., Hachet, O., Dalessi, S., Ullal, P., Bhatia, P., Bergmann, S., and Martin, S.G. (2015). Pom 1 gradient buffering through intermolecular auto-phosphorylation. *Molecular Systems Biology*, 7(11).

Hindmarsh, A.C., Brown, P.N., Grant, K.E., Lee, S.L., Serban, R., Shumaker, D.E., and Woodward, C.S. (2005). SUNDIALS: Suite of Nonlinear and Differential/Algebraic Equation Solvers. *ACM Transactions on Mathematical Software*, 31(3), 363–396.

Hock, S., Hasenauer, J., and Theis, F.J. (2013). Modeling of 2D diffusion processes based on microscopy data: parameter estimation and practical identifiability analysis. *BMC Bioinformatics*, 14 Suppl 1(Suppl 10), S7.

Hross, S. and Hasenauer, J. (2016). Analysis of cfse time-series data using division-, age- and label-structured population models. *Bioinformatics*.

Hug, S., Schwarzfischer, M., Hasenauer, J., Marr, C., and Theis, F.J. (2015). An adaptive scheduling scheme for calculating Bayes factors with thermodynamic integration using simpson's rule. *Stat. Comput.*

Kass, R.E. and Raftery, A.E. (1995). Bayes factors. *J. Am. Stat. Assoc.*, 90(430), 773–795.

Kazeroonian, A., Fröhlich, F., Raue, A., Theis, F.J., and Hasenauer, J. (2016). Cerena: Chemical reaction network analyzer - A toolbox for the simulation and analysis of stochastic chemical kinetics. *PLoS ONE*, 11(1), 1–15.

Martin, S.G. and Berthelot-Grosjean, M. (2009). Polar gradients of the DYRK-family kinase Pom1 couple cell length with the cell cycle. *Nature*, 459(7248), 852–856.

Moseley, J.B., Mayeux, A., Paoletti, A., and Nurse, P. (2009). A spatial gradient coordinates cell size and mitotic entry in fission yeast. *Nature*, 459(7248), 857–860.

Saunders, T.E. (2015). Aggregation-fragmentation model of robust concentration gradient formation. *Physical Review E*, 91, 022704.

Saunders, T.E., Pan, K.Z., Angel, A., Guan, Y., Shah, J.V., Howard, M., and Chang, F. (2012). Noise reduction in the intracellular pom1p gradient by a dynamic clustering mechanism. *Developmental Cell*, 22(3), 558–72.

Taheri-Araghi, S., Bradde, S., Sauls, J.T., Hill, N.S., Levin, P.A., Paulsson, J., Vergassola, M., and Jun, S. (2015). Cell-size control and homeostasis in bacteria. *Current Biology*, 25(3), 385–391.

Vyshemirsky, V. and Girolami, M. (2008). BioBayes: a software package for Bayesian inference in systems biology. *Bioinf.*, 24(17), 1933–1934.